Chapter 1

Introduction

1.1 INTRODUCTION

The concept of symmetry breaking is foremost to the study of condensed matter physics. A solid is composed of atoms bonded together in a distinct arrangement. The particular arrangement and the interactions between the atoms govern the properties of solids. The arrangement of atoms can occur in diverse quantum states emerging in crystalline solids, magnets, superconductors, metallic glasses, etc. These quantum states can be categorized on the premise of various symmetries that are broken. Symmetry breaking in these quantum states being one of the zenith of condensed matter physics in the previous century. Moreover, there was a new quantum state discovered in 1980, which does not result from symmetry breaking, known as the quantum Hall state [1]. The quantum Hall state exhibits in two-dimensional (2D) materials, in which majority of the sample is insulating in nature and currents are circulated along the edges only. The unidirectional edge currents are resistant to dissipation and promotes to the Quantum Hall Effect (QHE). The Quantum Hall State was the first state perceived to be *topologically* well defined from all prior states of matter. The outcome of the QHE is that the resistance being quantized absolutely in the units of e^2/h, independent of the material characteristics. The precise quantization of the Hall resistance stems from its topological emergence.

The geometrical properties of materials that are invariant under deformations has been widely studied under branch of mathematics so called Topology. A usual case of topological invariance is the shape of a coffee cup and a doughnut. Since both of these shapes having only one hole, a coffee cup can be simply deformed into the shape of a doughnut, as shown in figure 1.1, forming them topologically identical. However, an orange cannot be deformed into a doughnut, making them topologically well defined. Thus, the topological classification of shapes

pays no attention on the minor details and bear on the fundamental properties only, which persist consistent by deformations.
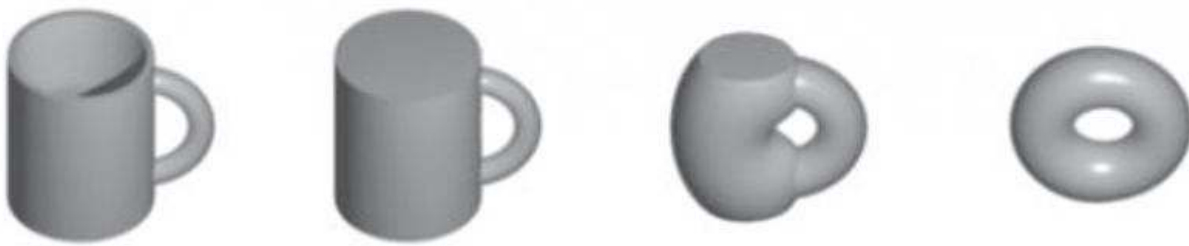
Comparably, the topological classification of solids in condensed matter physics, like the QHE impact on itself with the fundamental properties that remain invariant when the material or sample details are changed. Thus, the topological classification of quantum states bestows a powerful tool to interpret the fundamental properties of solids.

The topological classification in geometry is reasonable only for smooth deformations, without any violent actions, like tearing, etc. In physics point of view, such a 'smooth deformation' would be similar to the change in Hamiltonian of a many particle system, without closing the bulk band gap. Two quantum states are said to be topologically identical only if a smooth transition can arise from one state to the other without closing the band gap [2]. In the case of insulators, a topological classification would be valid only for the case where the band gap of the insulator is not closed. In other way, there exists a topological invariance that characterizes an insulator, which does not alter as long as the material persisting insulating property. Consequently, for the occurrence of a transition from a particular quantum state to another '*topologically*' well-defined quantum state, the band gap must approach to the transition point. The closing of the band gap is identical to the formation of conducting metallic states at

the interface. This notion leads to the origin of topological insulators (TIs), which is the objective of study for this thesis.

The prime technological attraction in TIs is their perspective application in spintronic devices. Spintronic devices store data based on the 'spin' state of an electron while transistors, which store data based on the charge state of an electron. The leading feature of TIs is the spin momentum locking of the topological surface state (TSS) which makes them promising candidates for spin-based devices. The spin momentum locking of the TSS is attributed to the large spin orbit coupling [3]–[5]. Spin orbit coupling (SOC) is the phenomena wherein the spin of a particle interacts with its motion, which can thus influence the band structure. SOC affects the band structure of all materials under study. In some materials, when the SOC is large, it can steer the p-band (valence band) to bend upwards and the s-band (conduction) to bend downwards, which can eventually lead to 'band inversion' while crossing each other. Substantially, if the band gap is small which the case in TIs, the effects of band inversion can be quite pronounced. The concept of band inversion is explained in significant detail in later.

The large SOC in TIs consequences to band inversion near the surface. The spin up and spin down electrons experience opposite effective fields, which propels them propagate in opposite directions. This phenomenon is known as spin momentum locking which reversing the current as well as spin state direction in a TI [6]. Based on the spin state of an electron, the spin momentum locking property can be utilized to store information which leads to spintronic device applications. The possibility of using TIs in spintronic devices for data storage is one of the prime inspirations for studying the detailed transport properties of TIs in this thesis.

Reversing the current direction in a TI leads to reverse the spin orientation as well. This exhibits two spin states (0 and 1) namely, depending on the directions of current flow and

electron spin, which can be used for information storage. The storing of information rely on electron spin instead of charge makes TIs as one of the most potential candidates for spintronic applications [7]. This thesis describes the fundamental transport properties of TIs, which is crucial for moving forward into device applications.

The absence of backscattering of the surface state electrons is one of the fundamental physical characteristic of TIs. The non-appearance of backscattering is a consequence of the spin momentum locking. There are no available spin states for the opposite current direction, hence no backscattering for the surface state. This characteristic makes TIs as attractive prospect for applications requiring very low dissipation like interconnects [8].

The spin momentum locking of the TSS along with low dissipation promotes to applications in quantum computing [9]. In order to perform operations on data, Quantum computing makes use of quantum mechanical phenomena like superposition and entanglement. The possible application of TIs for quantum computing applications makes it vital to understand the transport properties of TIs in detail. Thus, the large scope for applications in spintronic devices interconnects and quantum computing is the prime inspiration for studying the detailed transport properties of TIs in this thesis.

1.2: PHYSICS OF TOPOLOGICAL INSULATORS AND LITERATURE REVIEW

The band theory of solids developed in the 20th century defines an insulator as a solid elucidating an energy gap in the electronic band structure. The occurrence of the bandgap is a result of the periodicity of the crystal lattice and the entirely occupied atomic orbitals. The valence band of an insulator is thus entirely filled and separated from the empty conduction band. The bandgap of the insulator is generally defined as the difference between the valence and conduction band. The classification of solids based on the notion of a bandgap is significantly powerful idea, which prominently clarifies the study of solids in condensed matter physics.

The concept of topology derived from geometry can be utilized to further classify insulators [2]. The topological classification of solids is a substantial manner to study the band structures of insulators. It helps to understand the emergence of the diverse concepts which consequence to the existence of a topological insulator (TI) [7]. In order to receive an intuitive admiration of the topological classification of the band structure of an insulator, which exhibits a trefoil knot on the left hand side rendering the band structure of a TI and the circular loop on the right illustrating the band structure of an ordinary insulator or vacuum (See figure 1.2). Each insulator is distinguished based on a framework known as the *topological invariant*, which cannot alter as long as the material remains insulating [2]. Since the trefoil knot on the left side and the circular loop on the right side have different topological invariants, neither can be transformed into the other without cutting nor tearing. Hence, the knot must be cut at the interface, where the material transitions occur from a topological to a normal insulator. The cutting of the knot illustrates the *metallic state,* as shown by the figure in the middle. The quantity termed as wave function of an electron that is knotted in a TI. A metallic delocalized state must exist at the interface where the wave function is unknotted. Thus, transition occurring

from the topological to the normal state thus results in the formation of a metallic state at the interface, as illustrated by the 'cutting' of the knot. This promotes to an insulator with a *metallic surface*, known as a TI.
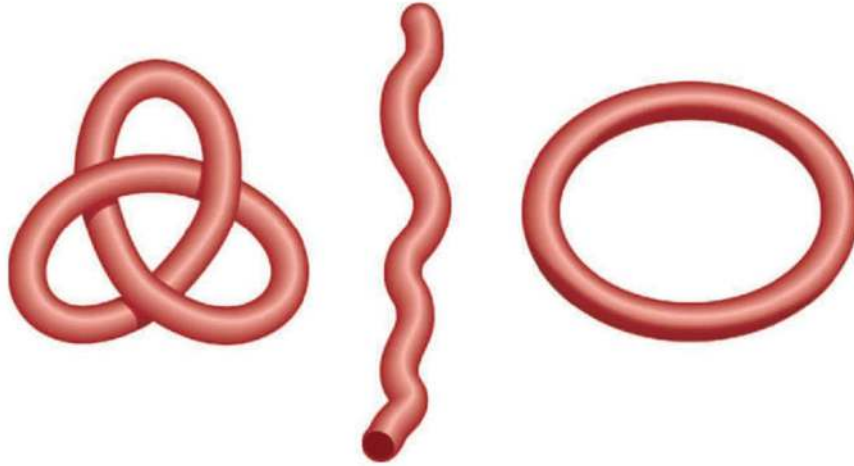

Figure 1.2: Topological change from a topological insulator to an ordinary insulator [2].

1.2.1: Physics of topological insulators

To be precisely interpret the cornerstone physics that propels topological insulators, it is essential to examine the Hall Effect and its many (quantized) siblings. These effects have been a pillar of condensed matter physics research for more than 100 years and persist an interesting and developing route of research. An overview of the `Hall effects' is shown in Table 2.1. It is worthwhile giving an overview of each, with particular emphasis focus on the quantum spin Hall Effect (QSHE) and quantum anomalous Hall effect (QAHE).

Table 1.1: Summary of the Hall effects and year of discovery for each

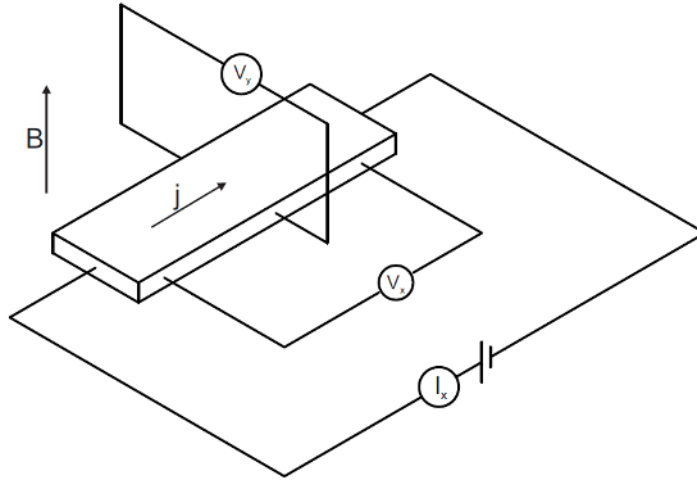| Hall Effect (1879)	Spin Hall Effect (1889)	Anomalous Hall Effect (2004)
Quantum Hall Effect (1980)	Quantum Spin Hall Effect (2006)	Quantum Anomalous Hall Effect (2013)

Figure 1.3: Typical geometry of the Hall Effect. Current (I_x) flows in plane, perpendicular to an applied field B inducing a mutually orthogonal potential V_x by action of the Lorentz force.

1.2.1.1 The Hall Effects

The Hall Effect may occur for a given sample with electrons traveling with respect to an applied magnetic field, with at least some velocity component being orthogonal to the field. For simplicity, one can assume the system as shown in Figure 1.3, where the electron velocity is perpendicular to the applied field. In this case, the Lorentz force will act on the electrons elucidated in Eq. 1.1, where $\vec{v}$ and $\vec{B}$ are the electron velocity and external applied magnetic field.

$$\vec{F} = -e\vec{v} \times \vec{B} \qquad (1.1)$$

This Lorentz force will evidently act in the third direction, orthogonal to applied field and electron velocity, resulting the owing electrons to travel a curved path through the sample. This in turn sets up an electric field ($\vec{E}_H$) defined by Eq. 1.2, where R_H and $\vec{j}$ are the Hall resistance and the current density, respectively.

$$\vec{E}_H = R_H \vec{B} \times \vec{j} \qquad (1.2)$$

In brief, a measurable potential is solicited across the sample by means of interaction of an external magnetic field and the charge carriers of the material, which leads to determine the Hall resistance RH. It is worthwhile to note that the Hall resistance allows a direct extraction of the electron density by the relation $R_H = -1/ne$, where e is the electron charge and n the carrier density. This argument is supported for electrons moreover, the same physics holds true for holes in p-type materials.

1.2.1.2: Quantum Hall Effect

The observation of first Quantum Hall Effect (QHE) was discovered by von Klitzing and well elucidated [10]. It is an effect observed in certain semiconducting materials under the influence of an applied external magnetic field. It can be considered in a similar fashion to the Hall Effect and can be used for the same sample geometry as previously outlined. A two dimensional electron gas (2DEG) may be esteemed as a sea of free electrons in 2 dimensions that are restricted by an `infinite' potential in the third. Under the low temperatures and high external magnetic fields, the electronic states in such a material (GaAs/AlGaAs) quantum wells for instance) will be confined to discrete Landau levels described by the Hamiltonian in Eq. 1.3.
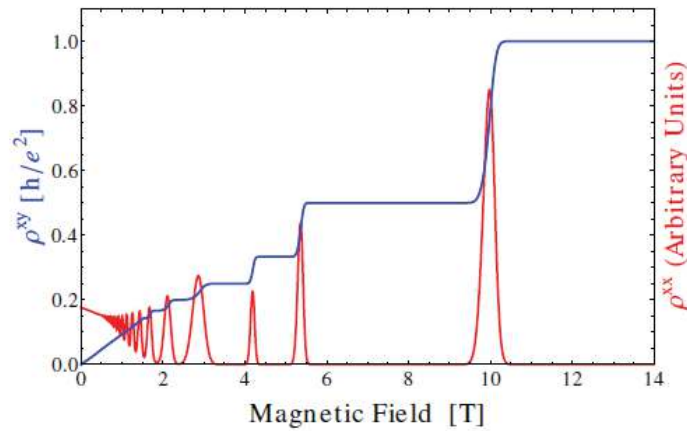

Figure 1.4: Transverse and longitudinal components or resistivity revealing the quantum Hall Effect for a GaAs-$Ga_{0.71}Al_{0.29}$ as heterostructure. ρ^{xy} shows quantization in units of h/ne^2 where n is an integer [10].

$$\hat{H} = \frac{\widehat{p_x^2}}{2m} + \frac{1}{2}m\omega_c^2\left(\hat{x} - \frac{\hbar k_y}{m\omega_c}\right)^2 \qquad (1.3)$$

Where H is the Hamiltonian operator, $\widehat{p_x^2}$ the momentum operator (in $\hat{x}$), m the mass (or effective mass), c is the electron cyclotron frequency, $\hat{x}$ is the position operator and k_y is the momentum in the $\hat{y}$ direction. From this it is straightforward to see by analogy with the harmonic oscillator that the electrons described by this Hamiltonian will form quantized energy levels with eigen values, where $n \geq 0$:

$$E_n = \hbar\omega_c\left(n + \frac{1}{2}\right) \qquad (1.4)$$

The electron energies are now quantized in units of w_c, their cyclotron frequency, which is itself a function of the applied external magnetic field, electron charge and mass ($\omega_c = eB/m$). From the basic principle, there are two main observable effects (shown in Figure 1.4): the vanishing of longitudinal resistivity and the quantization of transverse resistivity expressed as ($\rho^{xy} = -h/ne^2$) where n is an integer. A note worthy and detailed derivation is surpassing the scope of this thesis is emphasized and directed as per [10]. In brief, with increasing magnetic field, the energy separations of the Landau levels increases and electrons will occupy only the lowest energy levels up to the chemical potential. As the field increases, the occupation of the higher energy levels decreases as more electrons are accommodated in the lower Landau levels. The discrete changes in the quantization of resistivity takes place when an exact integer (n) Landau levels are filled, a state that occurs for each $B_n = n_A h/ne$, where n_A is the electron density. This discussion has been so far excluded to mention edge states, which can be explained semi-classically by consideration of the Lorentz force. An applied external magnetic field of sufficient strength will cause the bulk electrons to become localized within their cyclotron orbits and hence effectively

bulk insulating. Moreover, there will be some electrons for which their localized path causes them to the edge of the material. These edge electrons will `skip' along the interface creating a 1D channel of spin-polarized electrons at this edge. This state is illustrated diagrammatically in Figure 1.5. This is first example here of a topologically nontrivial bulk band structure driving a defined edge or surface state.
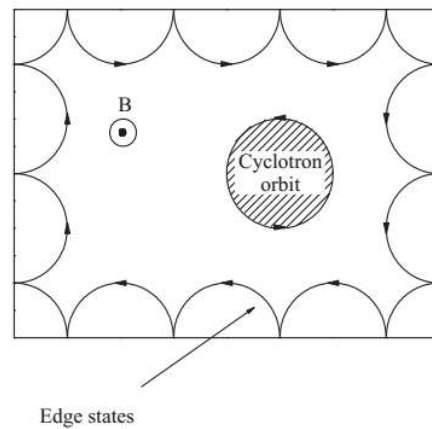

Figure 1.5: Diagrammatic picture of the electron localization into cyclotron orbitals leading to edge states.

This simplification is, of course, astonished since it considers only single electrons rather than bands. A thorough discussion must focus on the bending of the Landau level bands towards the edges of the sample, generating a confinement potential for the edge electrons.

1.2.1.3: Spin Hall Effect and Anomalous Hall Effect

Spin Hall (SH) and anomalous Hall (AHE) effects occur in the absence of an applied magnetic field in materials with strong spin-orbit interaction. The SHE [11] elucidates an accumulation of electrons of differing spin towards the edges of a current carrying sample, in a similar fashion to the Hall Effect causing gathering of differing charge. This effect is generally described by analogy to a spinning tennis ball, which deviates from its straight path, left or right,

depending on its spin causing a torque by interaction with the air. Likewise, an electron spin exerts a torque through the spin-orbit interaction.

The anomalous Hall Effect essentially replaces the applied external field of the Hall Effect with an internal magnetization, i.e., in a ferromagnetic material. It is detectable as an additional term to the Hall Effect, which is in general much larger than the `ordinary' Hall Effect. The end result will be a reversal in the sign of the measured Hall resistance (RH) for an equivalent reversal of the sample's net magnetization. This effect occurs again due to the spin-orbit interaction and can be considered as originating from intrinsic (Berry-phase curvature) and extrinsic processes. Examples of extrinsic processes are skew-scattering from impurities or side-jump scattering from impurities or electron-phonon interactions. A Brief in-depth discussion of this effect has been reported in Ref. [11].

1.2.1.4: Quantum Spin Hall Effect

The quantum spin Hall Effect (QSHE) is the solid foundation of the 2D topological insulators. Kane & Mele proposed a model for this effect [3] and it can be perceived in brief as a doubling of the previous model by incorporating the electron spin as up and down channels proposed by Haldane [12]. Given its importance to the remainder of this thesis, this effect will be discussed entirely within the context of topological insulators.

This discussion should begin by analysis of the similarities and differences between this and the QHE. The most notable difference being the absence of an applied field and by extension to that this state conserves the time-reversal symmetry (TRS). As in the QHE, one can divide a highway' across the sample. In the quantum Hall (QH) state electron channels for $+k_x$ and $-k_x$ are separated across the width of the sample (Figure 1.6[left]) and thus scattering is suppressed by this spatial separation.
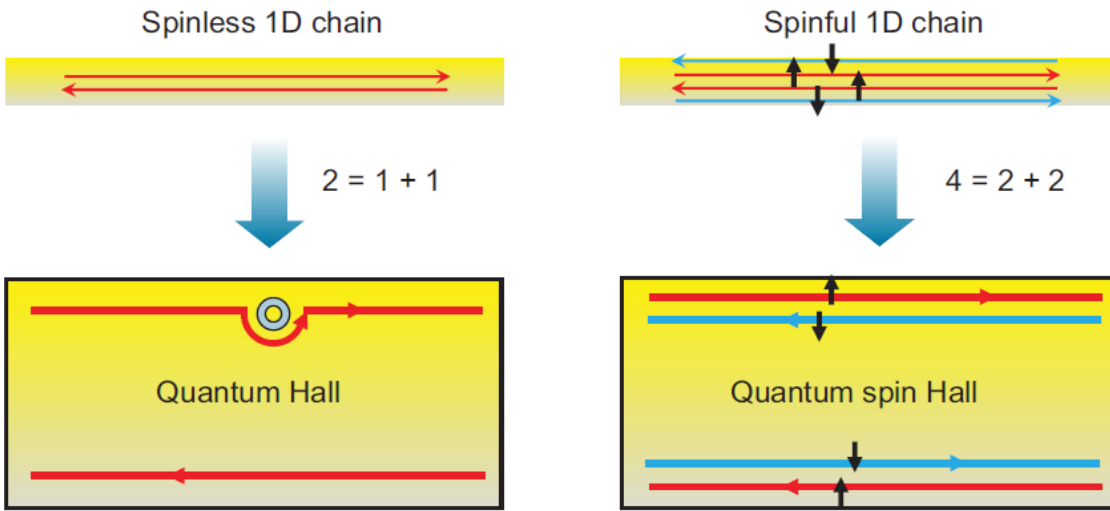
Figure 1.6: Left: QHE with both right-moving and left-moving edge states. These states are robust to scattering by impurities. Right QSHE with upper state right moving spin up and left-moving spin down. The lower state is inverted by comparison. Back-scattering is suppressed from non-magnetic impurities [13].

Note that in 1D, electrons may move in one of only two possible directions, this process would not suppress scattering in 2D. Figure 1.6 illustrates the dissipation less transport in this state since, on encountering an impurity, a given electron will detour around rather than back-scatter. Additionally in the Quantum Spin Hall state (QSH), the spin degree of freedom for the electron has been considered. This time-reversal invariant splitting of states does not require the application of an applied external field. Figure 1.6 [right] demonstrates the new setup with the 4-channel `divided highway' this state for bids back-scattering from non-magnetic impurities by goodness of some interference characteristics. Figure 1.7 demonstrates the case for a spin up electron encountering an impurity and back-scattering through two probable channels, each involving a continuous rotation about the impurity. The clockwise and anticlockwise path rotates the electron spin by π and $-\pi$ leading to a path difference of 2π. It is noteworthy to mention that the TRS of the state is crucial as it provides equal probability to each scattering path. Since spin-1/2 wave functions (Fermions) invert sign under a 2π rotation, these paths will destructively interfere, permitting for dissipation less transport of the electrons. This is essentially the similar
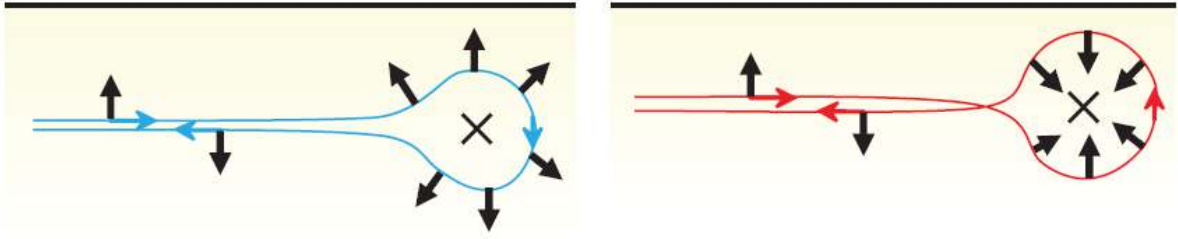
Figure 1.7: Diagrammatic depiction of the two different scattering paths around an impurity for the quantum spin Hall state. The total path difference between them is 2π, leading to total suppression of the back scattering for Fermions. Figure from Ref. [30].

mechanism by which anti-reflective coatings operate, squeezing destructive interference to suppress a scattering channel. If TRS is broken (by an applied field or magnetic impurity), this is no longer the case and back scattering may occur. Control of such a scattering process is of the vital important mechanism, as it is believed that TI-based devices may be built in future based on this phenomenon.

1.2.1.5: Spin orbit coupling

Spin orbit coupling (SOC) arises mainly due to the interaction of the electron spin or the intrinsic angular momentum of the electron with its orbital angular momentum. SOC is the leading property, which is mainly responsible for the formation of the Topological Surface States (TSS) and the spin momentum locking. In normal semiconductors, conduction band and valance band is formed from electrons in *s* and *p* orbitals, respectively. The *s* band (conduction band) bends upwards while the *p* band (valence band) bends downwards. Therefore, in ordinary materials, they never cross each other. However, SOC can result in inverting the band orientation of both s and p-bands. It may creating a band inversion in TIs, which is responsible for their unique properties. The detail explanation has been appended in below section. SOC affects the band structure of all materials. In those materials where the SOC is large, it can cause the p-band (valence band) to bend upwards and the s-band (conduction band) to bend downwards. Due to

the band bending, the s-band and the p-band can cross each other and the normal band structure gets 'inverted', thus promoting to 'band inversion' when they cross each other [5], [12]. Due to the band inversion mechanism, the s-band (conduction band) becomes lower in energy than the p-band (valence band). This unique state promotes to the occurrence of conducting states at the points where the bands intersect, which typically occurs at the surface. This leads to the closing of the band gap at the surface, resulting in the formation of the metallic surface states. When the SOC is quite large and the band gap is quite small (like in Bi_2Se_3), the effects of band inversion can be significantly enhanced. Thus, the band inversion gives rise to the metallic surface states or TSS.

Due to the large SOC, the spin up and spin down electrons at the TSS encounter opposite effective fields, which leads them to propagate in opposite directions. This phenomenon is known as spin momentum locking, which is the crucial property of TIs used for device applications. Due to the spin momentum locking effect the spin state also reverses as the current direction at the surface is reversed [7]. Thus, the spin orientation is governed by current direction. This fact can be implemented for applications in data storage, which entails the ability of easy switching property between two states.

One of the fundamental characteristic of spin momentum locking in TIs refers that the electron motion in any direction is preserved against back scattering [6], [13]. In order to understand the physics behind this process, a forward propagating spin-up electron is being considered. In case of a TI, the spin of the electron is locked to its momentum (shown in figure 1.8). Thus, in order to backscatter, the spin-up electron has to rotate to spin-down which is not possible due to lack of the opposite spin state required for backscattering. However, if the TR symmetry is broken (for example due to a magnetic impurity), backscattering can take place [13]. Thus, the principle of TR symmetry and spin momentum locking does not permit backscattering and preserves the robustness of the TSS.
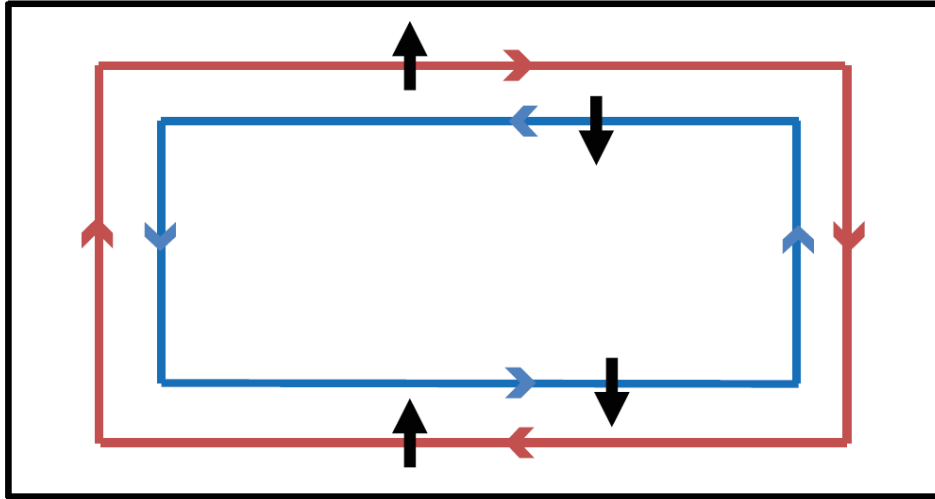
Figure 1.8: Helical edge states in the 2D TI

However, it is worthwhile to note that the above argument is viable only for an odd number of forward (or backward) moving channels. Backscattering can take place without rotating the spin in case of an even number of channels. Thus in order for TSS to be robust, there must be an odd number of forward and backward moving channels. This concept is expressed using the notion of a *Z2* topological quantum number[4]. In the following, experimental discovery of TIs has been discussed in detail.

1.3: EXPERIMENTAL DISCOVERY OF TOPOLOGICAL INSULATORS

1.3.1: First 2D topological insulator HgTe

It has been predicted the existence of the QSH state in HgTe quantum wells sandwiched between layers of CdTe by theoreticians [5]. This prediction was mould because of the strong SOC in HgTe, which results in a band inversion at the gamma point. This was a profound perception, which paved the way for the experimental realization of TIs. Furthermore, the strong lattice match between these materials results in a well formed CdTe/HgTe quantum well.
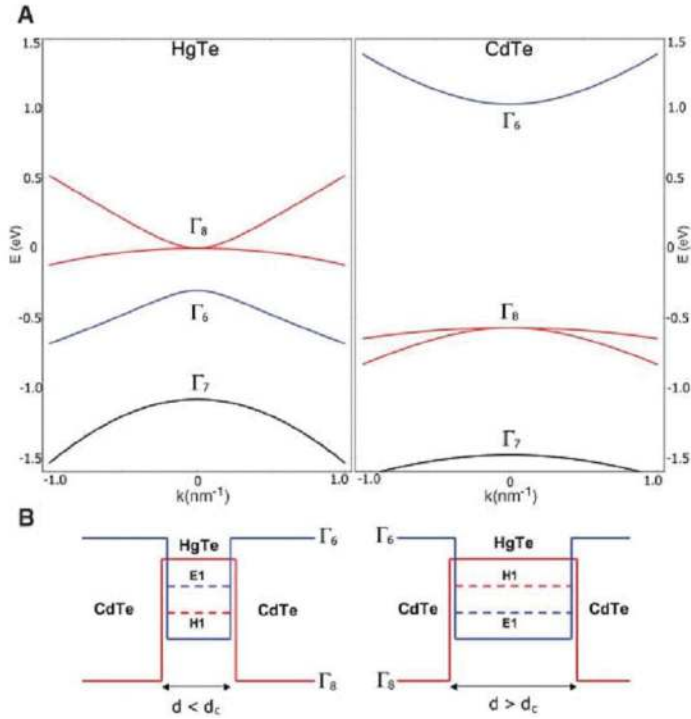
Figure 1.9: Band structure of CdTe/HgTe quantum well. Band inversion occurs when the well thickness is larger than the critical thickness [5].

Figure 1.9 shows the band diagram for the CdTe/HgTe quantum well structure. HgTe is a II-VI semiconductor. In most II-VI semiconductors, the conduction band comprises of s electrons derived from the group II atom whereas the valence band consists of the p electrons derived from the group VI atom, respectively. Moreover, in HgTe, this orderness is inverted, i.e. the conduction band contains the p electrons and the valence band contains the s electrons, if the HgTe quantum well thickness is greater than a critical thickness, the band structure within the well will remain inverted. According to the theoretical prediction, when the band structure is inverted, a QSH state appears resulting in dissipation less conductivity and spin polarized transport along the well interface. However, if the well thickness is less than the critical value, the CdTe band structure dominates with no band inversion and the structure behaves like a trivial insulator. The theoretical prediction was experimentally verified by the group led by Molenkamp in 2007, as shown in figure 1.10 [14].
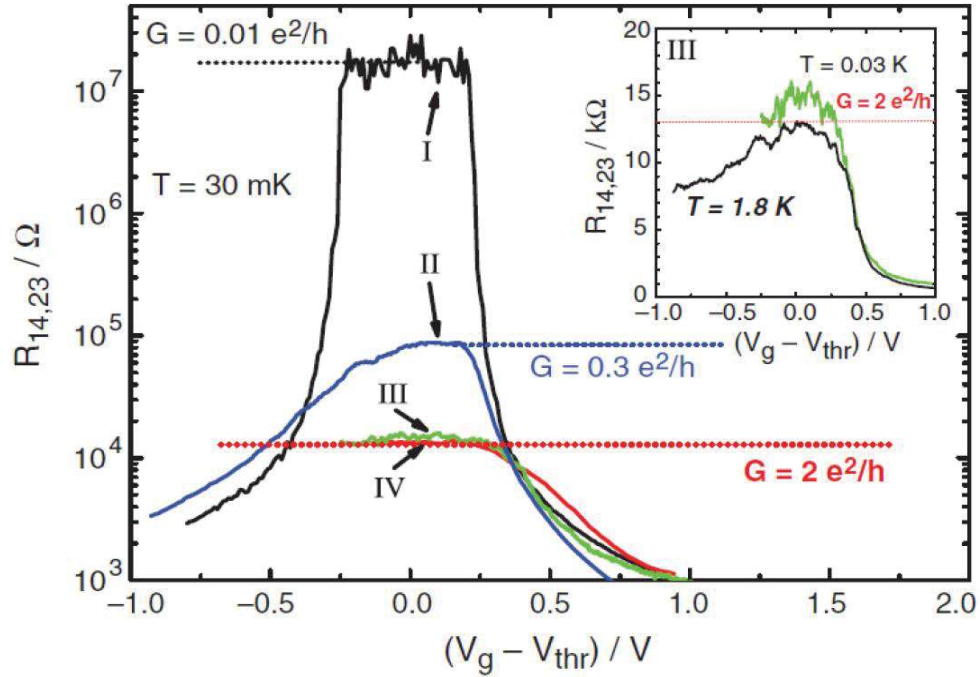
Figure 1.10: Experimental verification of TI behavior in CdTe/HgTe quantum well. The precise quantization of the current is confirmed by a conductance value of $2e^2/h$ [17].

In this pioneering experiment, the authors fabricated the CdTe/HgTe quantum well structures employing molecular beam epitaxy. The crucial idea is that when the thickness of the HgTe exceeds a critical value of 6.7 nm, band inversion occurs, leading to the appearance of the QSH state, with a characteristic conductivity of $2e^2/h$. When the thickness of HgTe is smaller than the critical thickness, it acts like a perfect insulator. This fact was experimentally verified in the transport experiment (as shown in figure 1.10), where the conductivity value is exactly $2e^2/h$, when the HgTe well thickness exceeds 6.7 nm (region III and IV), which clearly demonstrating the existence of the TSS at the well interface.

1.3.2: First 3D topological insulator $Bi_{1-x}Sb_x$

Although the experiment involving CdTe/HgTe quantum wells confirmed the existence of the QSH state in two dimensions, the demonstration of 3D TIs required angle resolved photoemission spectroscopy (ARPES) measurements. In contrary to the QH state which occurs

only for 2D systems, the QSH state was anticipated to occur even for 3D-systems [4]. The QSH

prediction for the 3D-system $Bi_{1-x}Sb_x$ was experimentally elucidated by Zahid Hassan's group

using ARPES [15]. Charge transport which was used to determine the 2D TIs are difficult in 3D

materials because of bulk effects, which makes it very tedious to identify the topological

signature of the surface states. ARPES is an ideal tool, which can be utilized to probe the

topological nature of the surface states. ARPES uses a photon to cause electron ejection from the

crystal to determine the surface and bulk electronic structures, by analyzing the momentum of

the ejected electron. ARPES grants us to isolate the surface states from the bulk band structure

because surface states do not disperse along a direction perpendicular to the surface, in contrast

to the bulk states [4]. A strong TI shows a linear dispersion relation in which the metallic surface

states intersect the Fermi level at an odd number of points. Figure 1.11 shows the ARPES

spectrum of $Bi_{1-x}Sb_x$, where five crossings of the surface state are visible. According to Kramer's

theorem, the degeneracy of states with an *odd number* of electrons exec time-reversal symmetry

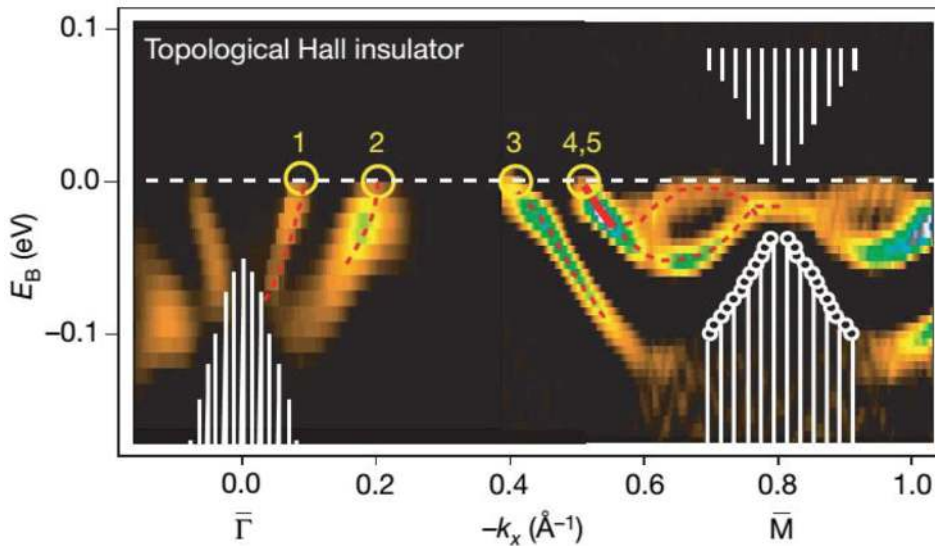is topologically protected [16] shown in figure 1.11.

Figure 1.11: The surface band dispersion second-derivative image of $Bi_{0.9}Sb_{0.1}$ along **Γ-M**. There are a total of 5 crossings between **Γ** and **M** which indicates topologically non-trivial surface states [19].

However, the TSS in $Bi_{1-x}Sb_x$ are quite complex in nature to analyze. Henceforth, it was predicted in 2009 that the compounds Bi_2Te_3, Bi_2Se_3 and Sb_2Te_3, having an easier band structure, could act as TI materials [17]. This was experimentally demonstrated later the same year using ARPES [18]. Figure 1.12 shows the ARPES spectrum of Bi_2Se_3, where the linear dispersion of the surface states is visible. It demonstrates the characteristic signature of a TI in the form of a single Dirac cone in the band structure.
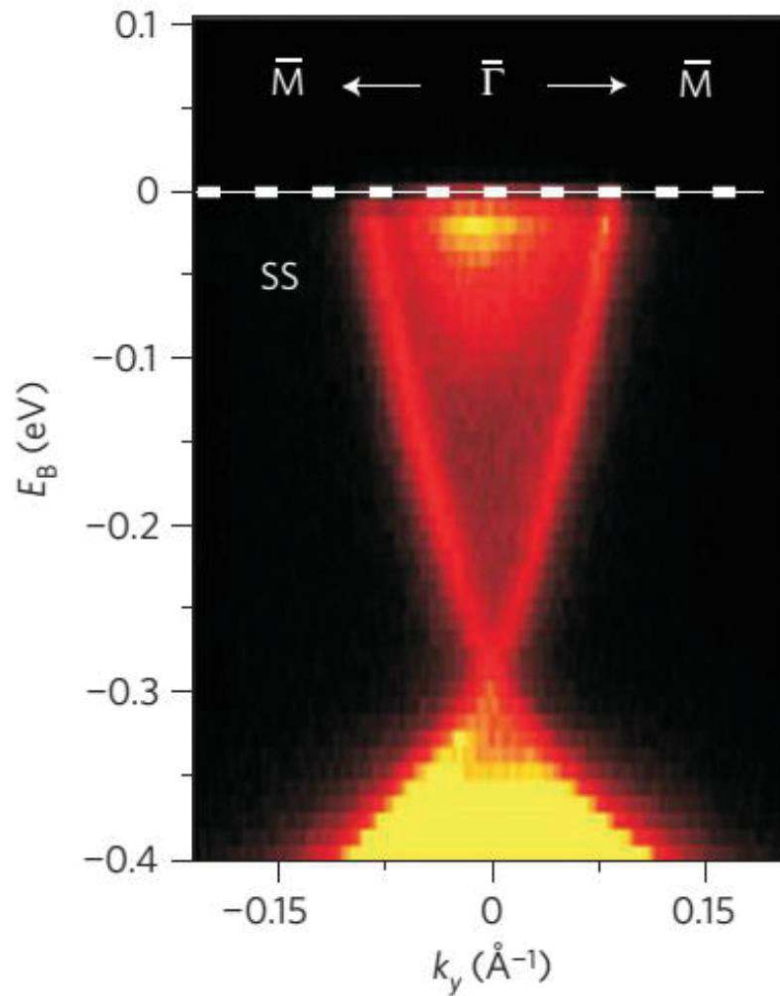
Figure 1.12: High resolution ARPES measurement of the surface electronic band dispersion on Bi_2Se_3 demonstrating the Dirac cone formed by the TSS [22].

Although Bi_2Se_3 is the most widely studied TI compound to date, it is not a perfect material and suffers from various defects, which can make the access to the TSS difficult in a

transport experiment. An insulator is defined by its band gap, which is approximately 0.3eV in Bi_2Se_3. Thus, at room temperature of 300 K (0.03eV), it should act as a reasonably good insulator. However, this assumption is true only if the Fermi level lies within the band gap. Ordinarily, Bi_2Se_3 grown in any form invariably contains Se vacancies, which act as dopants and push the Fermi level into the conduction band [19]–[24]. Due to the Fermi level lying inside the conduction band, the insulating Bi_2Se_3 begins to behave like a metal; this fact makes it extremely difficult to access the surface state due to the metallic-like nature of the bulk Bi_2Se_3. Thus, no clear signature of the TSS is visible at room temperatue in transport experiments using ordinary Bi_2Se_3 based compounds.

1.4: Bi_2Se_3 BASED MATERIALS FOR TIs

Bi_2Se_3 is the most widely studied TI material due to it simple band structure and well defined Dirac point. A lot of transport characterization studies have been done on Bi_2Se_3 in order to assess its suitability as a possible TI material for device applications. A thorough analysis of MBE grown Bi_2Se_3 films was done by Sean Oh's group at Rutgers [4]. They found that the Bi_2Se_3 films show a metallic behavior, but the carrier concentration and mobility is independent of temperature as shown in figure 1.13. They also observe a non-linear Hall signal, which indicates the presence of two types of carriers $Bi_2 (Se_xTe_{1-x})_3$ nano wires has been grown using chemical vapor deposition by Cui' group. One of the first works has been done by Ando' group ,
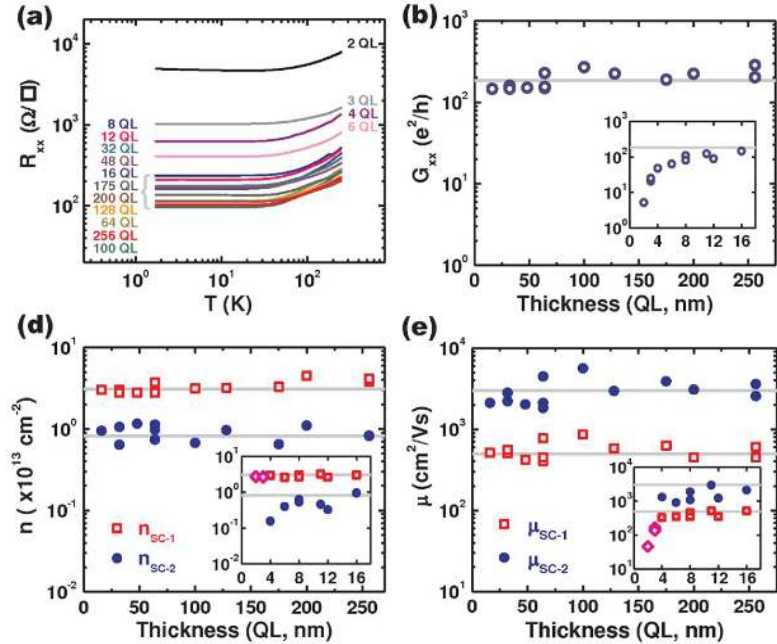
Figure 1.13: Characterization of MBE grown Bi_2Se_3 showing thickness independent behave employing chemical vapor deposition by Yi Cui's group at Stanford shows a strong weak anti-localization behavior with a large phase coherence length of ~200 nm, stipulating a significant surface state contribution, as shown in figure 1.13 [25].
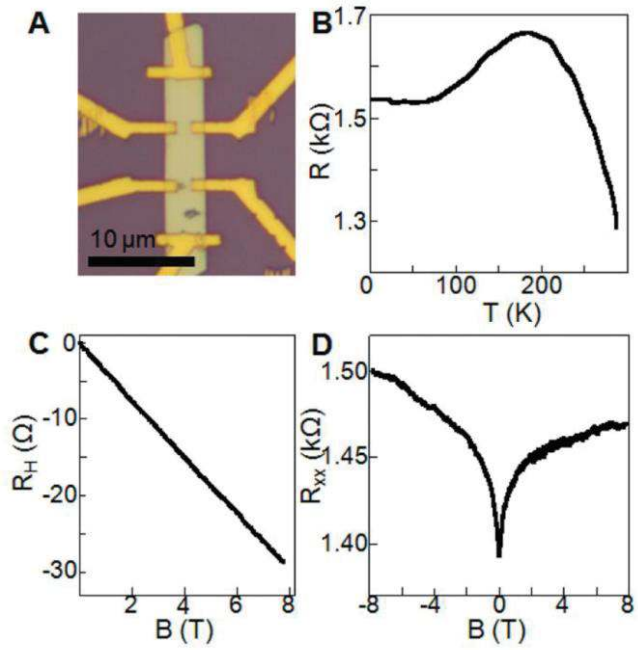

Figure 1.14: Transport characterization of $Bi_2(Se_xTe_{1-x})_3$ nanowires indicating strong weak anti-localization .

and his coworkers have reported their first study to reduce the contribution of the bulk channels

which used the single crystal quaternary alloy based on Bi-Sb-Te-Se (BSTS) to demonstrate an

insulating behavior from the bulk of the TI, as seen from the resistance vs. temperature plot of figure 1.15 [26]. However, the measurements were directly executed on bulk crystals without fabricating devices, making it tedious to implement in applications.
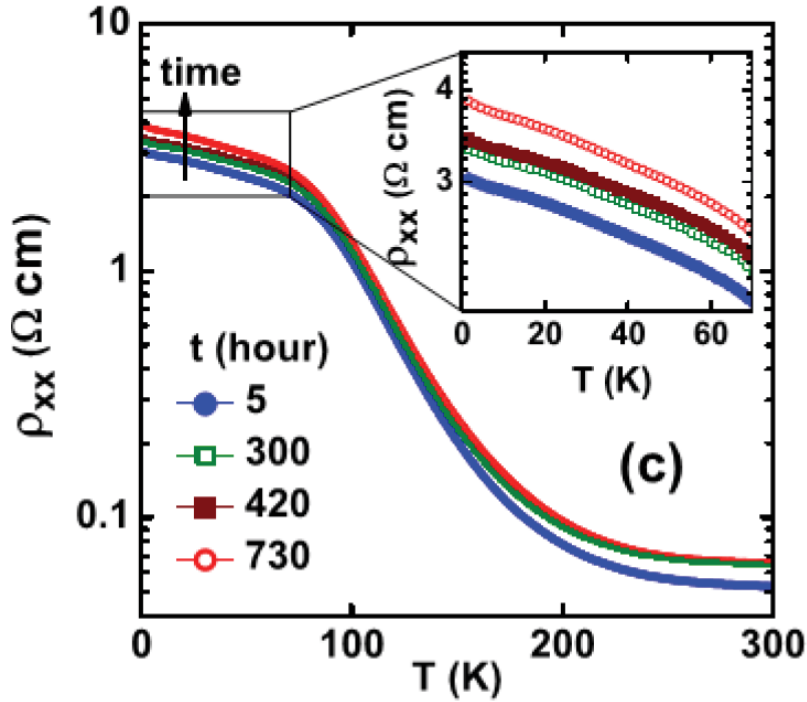

Figure 1.15: Bulk insulating behavior if BSTS by Ando group [30].

Currently, the research direction in TIs has shifted more towards applications in spintronic devices, which uses the spin momentum locking of the surface state. There have been recent experimental demonstrations of spin-momentum locking by in TIs[27], [28] The following section examines the spin momentum locking in TIs in detail.

1.5: SPIN MOMENTUM LOCKING IN TOPOLOGICAL INSULATORS

The large spin orbit coupling in TIs outcomes in the electron spin of the surface state to be locked perpendicular to its momentum. In k-space, this is comparable to the spin being

perpendicular to the *k*-vector. Figure 1.16 shows the spin texture of the TSS in *k*-space, elucidating the spin momentum locking direction of the top and bottom surfaces, respectively. The spin is locked in-plane and perpendicular to the momentum.
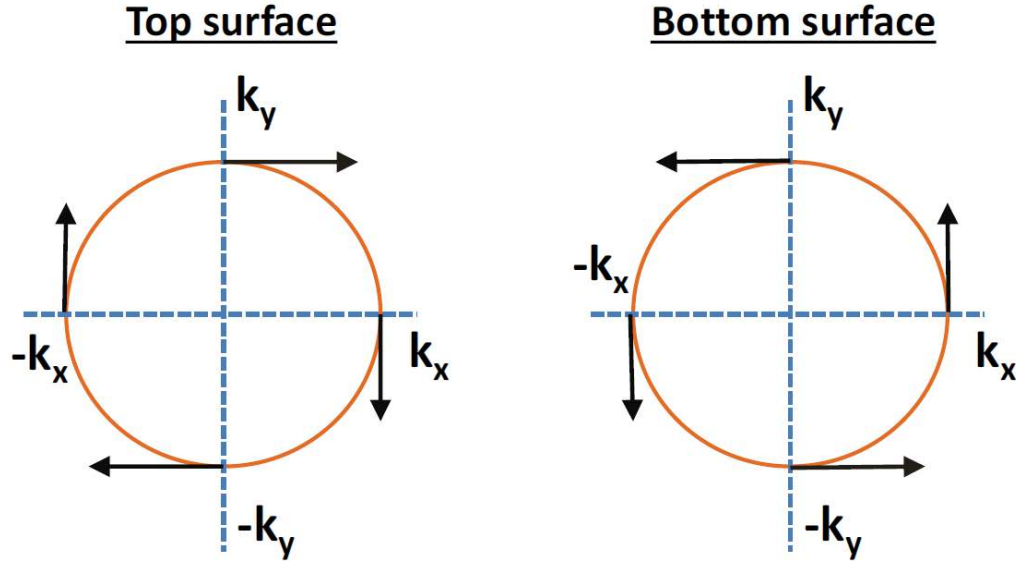

Figure 1.16: Spin texture in TI in k-space showing the spin momentum locking of the surface states.

1.5.1: First experimental demonstration of spin locking in Bi_2Se_3

The first experimental transport demonstration of the spin-momentum locking in Bi_2Se_3 was observed in 2014 [6]. In this experiment, since as a voltage signal measured on a ferromagnetic metal through a tunnel barrier used as the detector, it was demonstrated a direct electrical detection of the bias current-induced spin polarization in Bi_2Se_3. The uses of a ferromagnetic detector validate the authentic determination of the spin-polarization. The authors make use of two different ferromagnetic structures, namely Fe/Al_2O_3 and Co/MgO/graphene as the voltage detectors. The motivation behind the oxide layers is to banish any direct magnetic exchange interaction between the ferromagnet and the TSS. Figure 1.17 shows the device geometry and the measurement configuration as used by the authors.
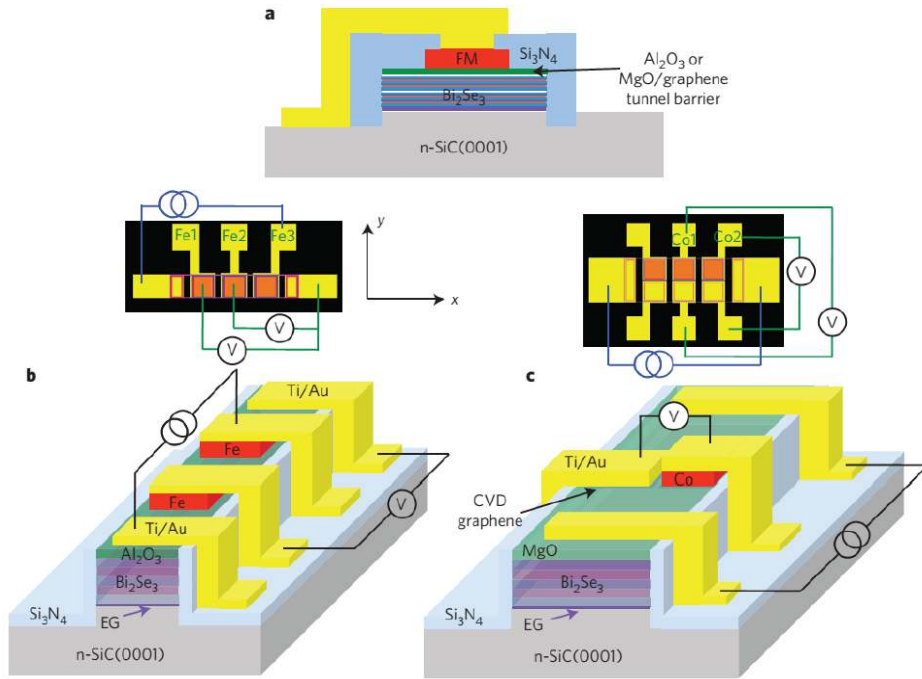
Figure 1.17: Device structure used for detecting spin momentum locking in TI. The use of a FM voltage detector enables detection of the current induced spin polarization of the TSS [7].

The basic idea behind the measurement technique is such that when the current flows through the Bi_2Se_3, and in-plane magnetic field perpendicular to the current direction applied, the spin of the TSS will align either parallel or anti-parallel to the magnetization of the ferromagnetic (FM) detector, because of the spin momentum locking property of the TSS. When the magnetic field is swept from the positive to the negative values, the magnetization of the FM detector will follow the field direction, depending on its coercively. Moreover, due to spin-momentum locking, the spin of the electrons in the TI will follow the current direction. Thus, when the magnetization of the FM detector reverses its sign, its alignment with respect to the spin direction of the TSS will change from parallel to anti-parallel. It is resulting in the occurrence of a hysteresis in the field sweep scan, as seen in figure 1.18(a-d). The observation of a hysteric switching behavior thus indicates the presence of the spin-polarization of the TSS. The

spin momentum locking of the TSS also reverses as reversing the current direction. As a consequence, when the current direction is reversed, the hysteric behavior will also reverse as seen in figure 1.18(a-c) and 1.18(b-d).
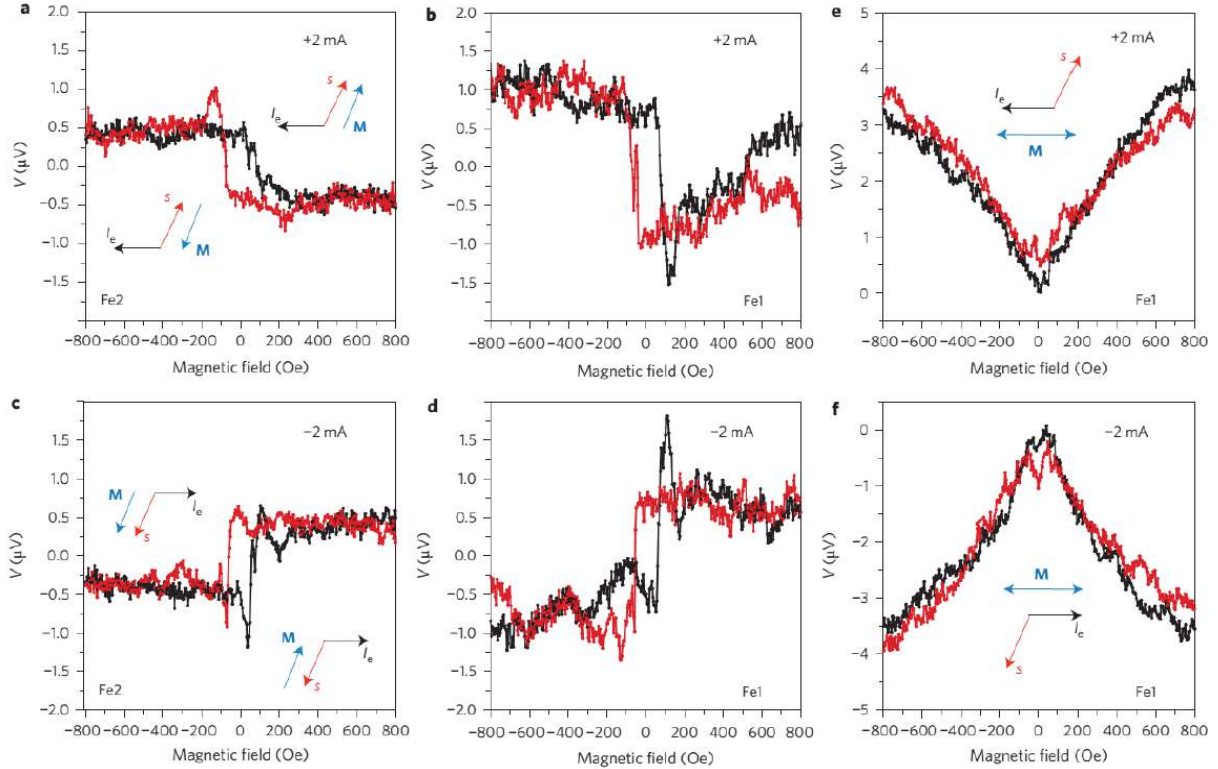

Figure 1.18: Voltage signal demonstrating the current induced spin polarization in TI. Obvious hysteresis is observed when the magnetic field is perpendicular to the current direction. The hysteresis signal is reversed on reversing the current direction. No hysteresis signal is observed when the external field is parallel to the current direction [7].

However, when the external field is parallel to the current direction, no hysteresis signal will be observed, as the spin of the TSS will remain perpendicular to the magnetization of the FM detector at all field values, as seen in figure 1.18 (e-f). These measurements instantly elucidated the spin-momentum locking property of the TSS. Similar reports by other groups have further justified the spin-momentum locking in TIs by electrical methods [29]–[32] locking signal However, there is no explicit agreement on the exact origin of the observed hysteresis signal. Recently, there was a report elucidating that the observed spin-momentum can occur from

fringe field induced Hall voltages [32]. In their report, in order to obtain similar hysteretic loops to the previous studies, the authors suggest a novel device geometry which comprises of a Hall bar patterned geometry with ferromagnet detector [6], [28], [30], [31] The authors used the device design with enabled additional design flexibility accrediting the decoupling of the spin and current paths which provides a distinctive prospect to explore additional magneto resistive effects arising in the TI channel which could lead to the observed signal behavior. Unexpectedly, the authors acquired a hysteresis signal in the measurement when the external field was parallel to the current direction, for which no spin locking hysteretic signal is anticipated. Authors also obtain alike hysteresis signal for the external field perpendicular to the current direction as well, as presumed TI spin locking. From these investigations, it is evident that the voltage signal obtained when the applied field is parallel and perpendicular to the current direction reveals features, which cannot be accredited to the spin polarization solely. It is also observed that similar characteristics can result from Hall voltages originated by the fringe fields from the FM detector in proximity to the TI channel. The device geometry and observed signal used in this study is shown in figure 1.19.
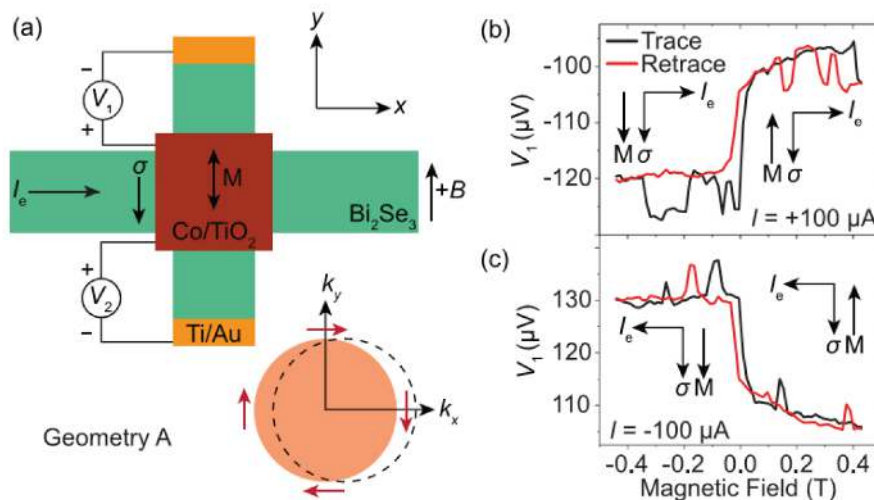

Figure 1.19: The device structure and measurement geometry for TI channel with FM detector demonstrating the signal corresponding to the current induced spin polarization of the TSS [37].

These fringe fields are available for all the different measurement geometries promotes to the development of local Hall voltages perpendicular to the current due to the small geometrical misalignment of the contacts. The existence of the fringe field induced voltages available in all measurement geometries specify that it may be incorrect to entirely attribute the observed voltage signal to the current induced spin polarization of the TI channel. These findings propel a shadow of uncertainty to the elucidation of the observed signals in the transport experiments revealing the spin momentum locking of the TI. These observations thus demands a new experimental efforts and more cautious interpretation of voltage signals in transport experiments demanding TI and FM heterostructures.

1.5.2: Magnetization switching using topological insulators

An electrical measurement, which demonstrated the existence of the TSS, the further insightful question arises whether the spin-polarization of the TSS can be used to switch a ferromagnet (FM)? The answer emerges to be yes as evidenced in 2014 by Kang Wang's group[33]. In this work, the authors demonstrate the switching of the magnetization of Cr-doped TI film $(Cr_{0.08}Bi_{0.54}Sb_{0.38})_2Te_3$, which functions as the FM layer, using the spin-polarized current flowing through the TI $(Bi_{0.5}Sb_{0.5})_2Te_3$, as shown in figure 1.20. The elucidation of switching can promote to exciting applications of TIs in spintronic devices.
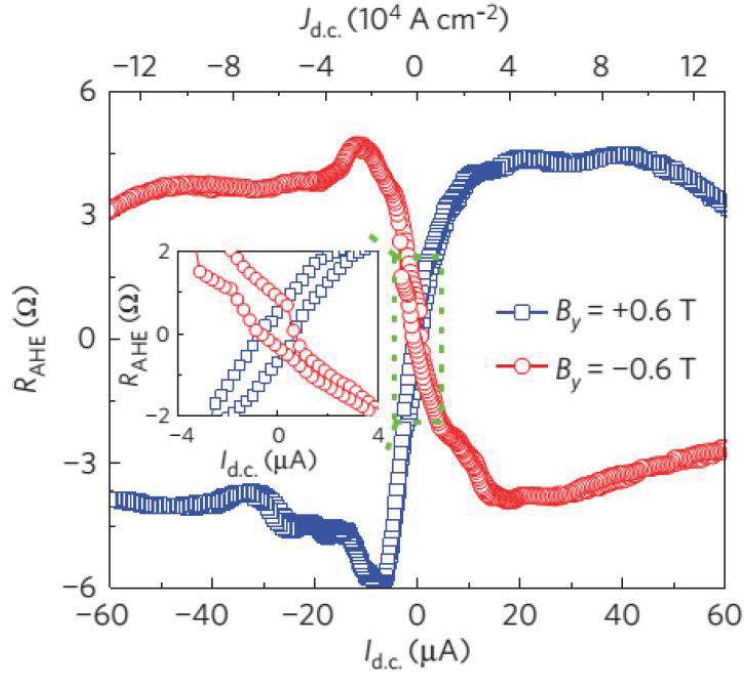
Figure 1.20: Current induced magnetization switching in $(Bi_{0.5}Sb_{0.5})_2Te_3/(Cr_{0.08}Bi_{0.54}Sb_{0.38})_2Te_3$ heterostructure at constant in-plane external field of 0.6 T and -0.6 T [38].

1.6: BROKEN TIME REVERSAL SYMMETRY

It should be understandable that TRS is a fundamental part, which makes a topological insulator an interesting material. Therefore, it is of appeal, to account what happens in the case when this symmetry is broken and the kind of process involved in breaking.

In general, broken symmetry is widely studied area of physics and within condensed matter that has been utilized extensively as a tool for the classification of materials, notably that of crystals. An ideal example of such phenomena is the phase transition between water and ice. Water exhibits full translational and rotational symmetry. Undergoing transition to ice breaks this symmetry, which results only rotational and translational invariant along defined directions within the crystal.
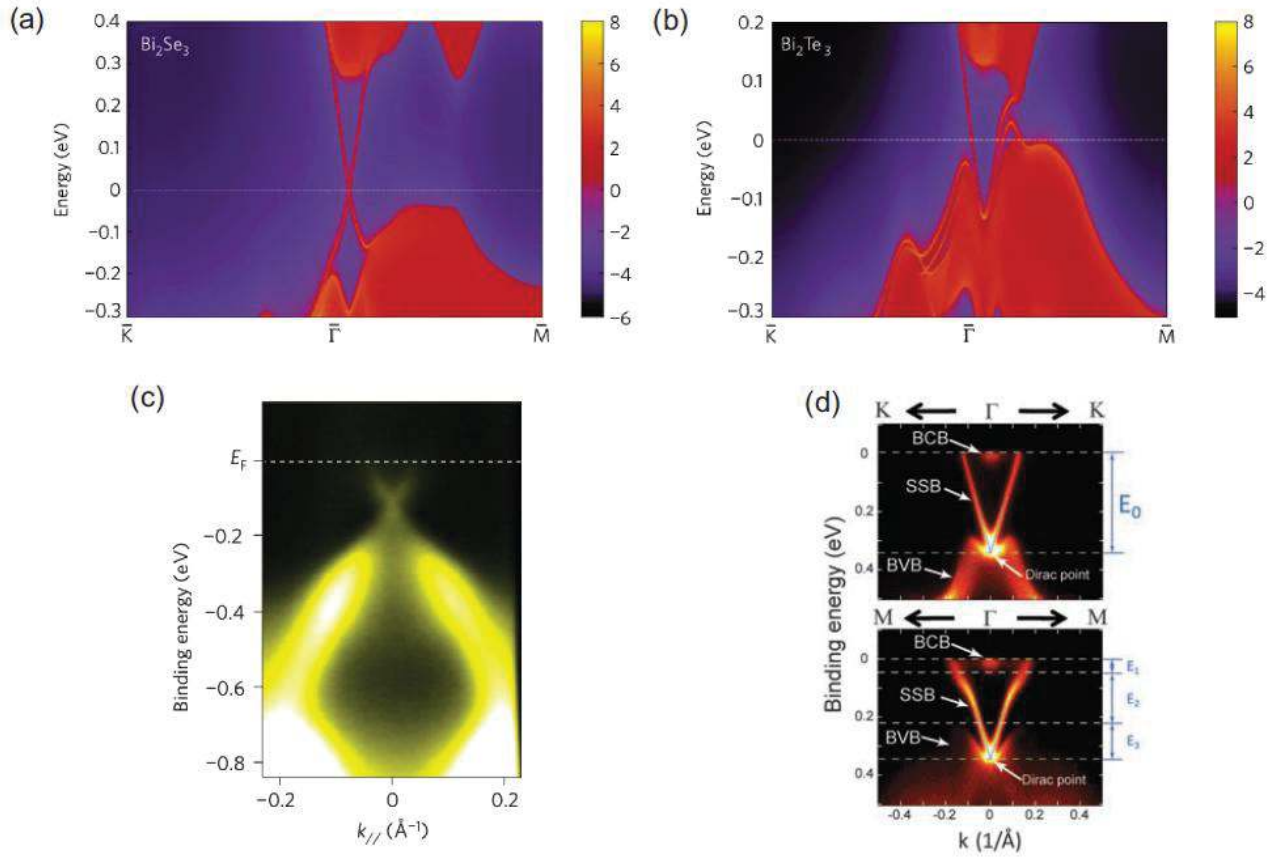
Figure 1.21: (a), (b) Band structure calculations of Bi_2Se_3 and Bi_2Te_3 respectively, showing the Dirac point crossing at 0 momentum [34][39]. (c) ARPES of Bi_2Se_3 showing Dirac point in the band dispersion [35][40]. (d) ARPES of Bi_2Te_3 similarly showing the Dirac band dispersion [36] [41].

Thus, the breaking of symmetry offers a precise way of distinguishing phases of matter and assisting phase transitions. A gap will open in the topological surface state under the application of a TRS-breaking action such as out of plane magnetic fields or ferromagnetic order [14]. This transition is then occurs between the band structure of a massless to a massive Dirac Fermion. A Dirac Fermion defined as a fermion that is not having its own antiparticle, exhibits a dispersion relation elucidated by a Dirac cone, like in the TSS. Similar to the standard formulation for semiconductors, the mass described here is an effective mass, related to the direct band gap. This effect has been first observed in Bi_2Se_3 doped with magnetic elements, which initiates an opening of the surface bands (Fig. 1.22) [37].
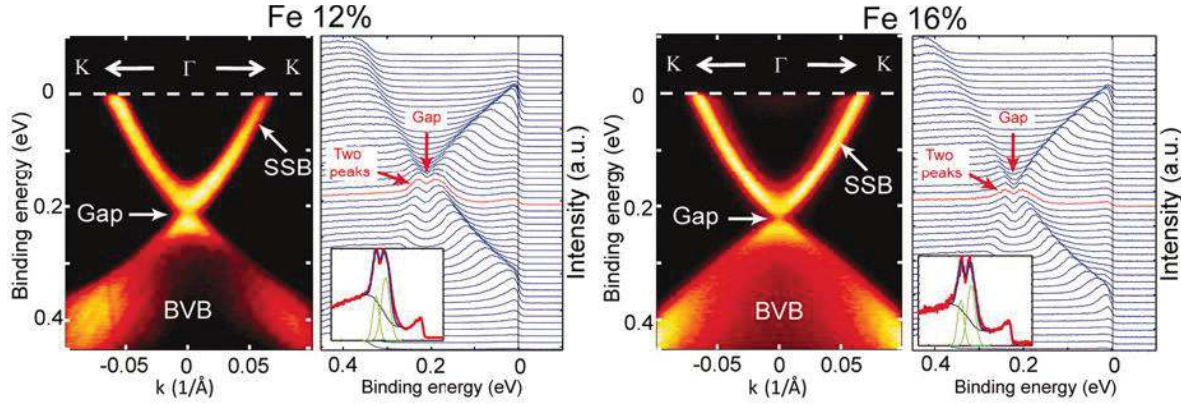
Figure 1.22: Bi_2Se_3 doped with varying levels of Fe in the bulk of the film. A gap-opening at the gamma-point is seen as a function of doping.

This doping will break TRS for either bulk ferromagnetism obtained through homogeneous doping or for exclusive surface ferromagnetism mediated through the RKKY interaction.

It is believed that control of these massive Dirac Fermion states may promotes to the discovery of new physical aspects and assisting breakthroughs in spintronic and quantum computation. For example, with a massive Dirac Fermion with EF tuned into the surface band gap, one may see the image magnetic monopole [38].

1.7: CONCLUSION

In this chapter, the physics of TIs was discussed in detail. The QHE was introduced as the first state, which does not involve symmetry breaking with a topological classification of the edge currents, and the TSS was revealed similar to the QH state. The key physical properties of TIs like spin momentum locking and absence of backscattering was discussed, and the first experimental realization of TIs was introduced. Finally, a brief review of the experimental progress in TIs was presented, including the first electrical measurement of spin momentum locking in Bi_2Se_3.